# The electronic structure and bonding of AlNAl

Apostolos Kalemos[a] and Aristides Mavridis[b]
*Laboratory of Physical Chemistry, Department of Chemistry, National and Kapodistrian University of Athens, P.O. Box 64 004, 157 10 Zografou, Athens, Greece*

(Received 2 February 2009; accepted 5 March 2009; published online 16 April 2009)

We have studied 16 states, 7 doublets, and 9 quartets of the AlNAl isomer mainly through multireference methods and correlation consistent basis sets. We report equilibrium geometries, energetics, and dipole moments, whereas for a number of low lying states we have constructed dissociation AlN–Al potential energy profiles. For the same states we also analyze their bonding character using valence–bond–Lewis diagrams. Our results are consistent with the limited experimental data. © *2009 American Institute of Physics*. [DOI: 10.1063/1.3106614]

## I. INTRODUCTION

The first experimental observation of the AlNAl molecule was made for the first time through Knudsen effusion mass spectrometry in 1970 by Gingerich, who determined its atomization enthalpy $\Delta_a H_0^0(g)=822\pm21$ kJ/mol ($=196.5\pm5$ kcal/mol).[1] Thirty years later Meloni and Gingerich redetermined this value to $\Delta_a H_0^0(g)=783.2\pm15$ kJ/mol ($=187.2\pm3.6$ kcal/mol).[2] The same year Andrews *et al.* recorded the infrared spectra of AlNAl in frozen argon matrices,[3] reporting symmetric and asymmetric frequencies $\omega(\mathrm{ss})=544.9$ and $\omega(\mathrm{as})=956.7$ cm$^{-1}$, respectively. Finally, Neumark and co-workers measured for the first time the adiabatic electron affinity EA $=2.571\pm0.008$ eV of AlNAl and obtained (indirectly) the two lowest electronic transitions, namely, $T_e(\tilde{A}\,^2\Pi_u \leftarrow \tilde{X}\,^2\Sigma_u^+)=5570\pm970$ cm$^{-1}$ and $T_e(\tilde{B}\,^2\Sigma_g^+ \leftarrow \tilde{X}\,^2\Sigma_u^+)=10\,490\pm970$ cm$^{-1}$, by negative ion photoelectron spectroscopy.[4]

On the theoretical side the only calculations in the literature are of the density functional theory (DFT) type, based on the B3LYP (Refs. 2–5) and BPW91 (Ref. 6) functionals.

Motivated by the complete lack of *ab initio* results on AlNAl and as a continuation of our work on the diatomic AlN (Ref. 7) and the isovalent BNB species,[8] we have investigated, mainly by multireference variational methods, the electronic structure of 16 bound AlNAl states within an energy range of ~4 eV.

For both Al and N atoms the correlation consistent basis set of quadruple cardinality (cc-pVQZ) was used, generally contracted to $[6s5p3d2f1g/_{\mathrm{Al}}5s4p3d2f1g/_{\mathrm{N}}]$.[9] When calculating the adiabatic electron affinity of AlNAl, the cc-pVQZ basis was augmented by a series of diffuse Al (Ref. 9) and N (Ref. 10) functions resulting to the contracted set $[7s6p4d3f2g/_{\mathrm{Al}}6s5p4d3f2g/_{\mathrm{N}}]$.

The complete active space self-consistent field (CASSCF) reference wave functions were constructed by distributing the 11 "active" electrons, $(3s^23p^1)\times2+2s^22p^3$, in the 12 orbital valence functions under $C_{2v}$ or $C_s$ constraints. The size of the CASSCF spaces range from about 70 000 (quartets) to 85 000 (doublets) configuration functions (CF) under $C_{2v}$ or twice this size under $C_s$ symmetry constraints. "Dynamical" correlation was extracted through single and double replacements out of the zeroth order functions (CASSCF+1+2=MRCI) and within the internally contracted (ic) scheme, as implemented in the MOLPRO suite of codes.[11] The icMRCI expansions contain about $17\times10^6$ ($C_{2v}$) or $34\times10^6$ ($C_s$) CFs. For the $\tilde{X}\,^2\Sigma_u^+$ and $\tilde{a}\,^4B_2$ states of AlNAl and the $\tilde{X}\,^1\Sigma_g^+$ states of the AlNAl ions, $\mathrm{AlNAl}^{\pm}$, the coupled-cluster+singles+doubles+semiperturbative connected triples [RCCSD(T)] methodology was also employed.[12]

For all states we report total energies, geometries, and (expectation value) dipole moments; in addition for the states $\tilde{X}\,^2\Sigma_u^+$, $^2\Pi_u(\tilde{A}\,^2A_1,\ \tilde{B}\,^2B_1)$, $\tilde{C}\,^2\Sigma_g^+$, $\tilde{a}\,^4B_2$, and $\tilde{F}\,^2\Pi_g$ we have constructed AlN–Al potential energy curves (PEC).

## II. RESULTS AND DISCUSSION

We have studied seven doublets [$\tilde{X}\,^2\Sigma_u^+$, $^2\Pi_u(\tilde{A}\,^2A_1,\ \tilde{B}\,^2B_1)$, $\tilde{C}\,^2\Sigma_g^+$, $\tilde{D}\,^2A_1$, $\tilde{E}\,^2A_1$, $\tilde{F}\,^2\Pi_g$] and nine quartets ($\tilde{a}\,^4B_2$, $\tilde{b}\,^4B_1$, $\tilde{c}\,^4A_1$, $\tilde{d}\,^4\Sigma_g^+$, $\tilde{e}\,^4\Delta_g$, $\tilde{f}\,^4\Sigma_g^-$, $\tilde{g}\,^4\Delta_u$, $\tilde{h}\,^4\Sigma_u^-$, $\tilde{i}\,^4\Pi_g$); numerical results for all these states ($E$, $r_e$, $\sphericalangle\mathrm{AlNAl}=\theta_e$, $\mu_e$, $T_e$) are given in Table I. Figure 1 displays dissociation AlN–Al profiles of the $\tilde{X}\,^2\Sigma_u^+$, $^2\Pi_u$, $\tilde{C}\,^2\Sigma_g^+$, $\tilde{a}\,^4B_2$, and $\tilde{F}\,^2\Pi_g$ states.

In what follows we discuss in some detail the structure and bonding of the $\tilde{X}\,^2\Sigma_u^+$, $\tilde{A}\,^2A_1$, $\tilde{B}\,^2B_1$, $\tilde{C}\,^2\Sigma_g^+$, $\tilde{a}\,^4B_2$, and $\tilde{F}\,^2\Pi_g$ states; for the rest of the states we simply comment upon our numerical findings.

### A. States $\tilde{X}\,^2\Sigma_u^+$, $\tilde{A}\,^2A_1$, $\tilde{B}\,^2B_1$, $\tilde{C}\,^2\Sigma_g^+$, $\tilde{a}\,^4B_2$, and $\tilde{F}\,^2\Pi_g$

In accordance to experimental[4] and DFT (Refs. 3 and 4) results our calculations corroborate beyond any doubt that the ground state of AlNAl is of $^2\Sigma_u^+$ symmetry. The AlNAl can be thought of as being formed by a linear attack of

[a]Electronic mail: kalemos@chem.uoa.gr.
[b]Electronic mail: mavridis@chem.uoa.gr.

 

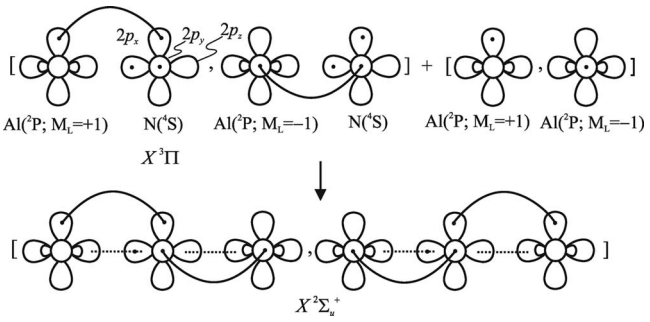


$Al(^2P)$ to the ground state of $AlN(X\ ^3\Pi)$.[7] The process and bonding can be succinctly captured by the above valence–bond–Lewis (vbL) icons.

Notice that the pair icons of AlN, Al ($M_L = \pm 1$), and of the product AlNAl are required to describe correctly the *ungerade* ($u$) symmetry of the $\tilde{X}\ ^2\Sigma_u^+$ state. According to the above diagrams the bonding of the $\tilde{X}\ ^2\Sigma_u^+$ state comprises two three-center two-electron ($3c\text{-}2e^-$) completely delocalized $\pi$ bonds and a one-electron delocalized $\sigma$ bond. The identity of the two N–Al bonds precludes any symmetry breaking effect. It is interesting to recall at this point the structure of the isovalent BNB molecule, whose ground state is also of $^2\Sigma_u^+$ symmetry, the result of the $BN(X\ ^3\Pi) + B(^2P;\ M_L = \pm 1)$ interaction.[8] However, the suggested asymmetric structure (symmetry broken) of the $\tilde{X}\ ^2\Sigma_u^+$ BNB species,[13–16] but strongly disputed,[8] has a completely different bonding character than that of AlNAl. For one thing, one

TABLE I. Total energies $E$ ($E_h$), geometries $r_e$ (Å) and $\theta_e$ (degrees), dipole moments $\mu_e$ (Debye), and separation energies $T_e$ ($cm^{-1}$) of AlNAl at the MRCI(+$Q$) level.

| State | $-E$ | $r_e$ | $\theta_e$ | $\mu_e$ | $T_e$ |
|---|---|---|---|---|---|
| $\tilde{X}\ ^2\Sigma_u^+$ | 538.650 62 | 1.7350 | 180.0 | 0.0 | 0.0 |
| | (0.668 0) | | | | (0.0) |
| | 538.667 37[a] | 1.7288[a] | 180.0[a] | 0.0 | |
| | 539.299 35[b] | 1.7199[b] | 180.0[b] | 0.0 | |
| $\tilde{A}\ ^2A_1$ [c] | 538.628 23 | 1.7997 | 128.82 | 0.265 | 4 914 |
| | (0.645 5) | | | | (4 938) |
| $\tilde{B}\ ^2B_1$ [c] | 538.625 01 | 1.8384 | 180.0 | 0.0 | 5 621 |
| | (0.642 9) | | | | (5 509) |
| $\tilde{C}\ ^2\Sigma_g^+$ | 538.605 74 | 1.7154 | 180.0 | 0.0 | 9 850 |
| | (0.623 3) | | | | (9 811) |
| $\tilde{a}\ ^4B_2$ | 538.568 32 | 1.8116 | 90.76 | 1.66 | 18 063 |
| | (0.586 6) | | | | (17 865) |
| | 538.583 72[d] | 1.8109[d] | 90.88[d] | 1.67[d] | 18 359[d] |
| $\tilde{D}\ ^2A_1$ | 538.558 22 | 1.7892 | 91.89 | 2.55 | 20 279 |
| | (0.577 1) | | | | (19 950) |
| $\tilde{E}\ ^2A_1$ | 538.544 61 | 1.7538 | 111.74 | 1.42 | 23 267 |
| | (0.569 3) | | | | (21 662) |
| $\tilde{b}\ ^4B_1$ [e] | 538.541 84 | 1.7321 | 141.12 | 1.12 | 23 874 |
| | (0.556 8) | | | | (24 406) |
| $\tilde{c}\ ^4A_1$ [e] | 538.540 74 | 1.7098 | 180.0 | 0.0 | 24 116 |
| | (0.555 0) | | | | (24 801) |
| $\tilde{F}\ ^2\Pi_g$ | 538.538 72 | 1.7234 | 180.0 | 0.0 | 24 559 |
| | (0.558 3) | | | | (24 076) |
| $\tilde{d}\ ^4\Sigma_g^+$ | 538.531 85 | 1.8308 | 180.0 | 0.0 | 26 067 |
| | (0.550 6) | | | | (25 766) |
| $\tilde{e}\ ^4\Delta_g$ | 538.523 95 | 1.8345 | 180.0 | 0.0 | 27 801 |
| | (0.543 8) | | | | (27 259) |
| $\tilde{f}\ ^4\Sigma_g^-$ | 538.518 50 | 1.8372 | 180.0 | 0.0 | 28 997 |
| | (0.538 4) | | | | (28 444) |
| $\tilde{g}\ ^4\Delta_u$ | 538.514 73 | 1.8270 | 180.0 | 0.0 | 29 824 |
| | (0.534 9) | | | | (29 212) |
| $\tilde{h}\ ^4\Sigma_u^-$ | 538.507 43 | 1.8278 | 180.0 | 0.0 | 31 427 |
| | (0.527 9) | | | | (30 748) |
| $\tilde{i}\ ^4\Pi_g$ | 538.490 88 | 1.7165 | 180.0 | 0.0 | 35 059 |
| | (0.516 3) | | | | (33 294) |

[a]RCCSD(T) results based on Hartree–Fock (HF) orbitals; based on CASSCF orbitals the corresponding numbers are −538.667 55 $E_h$ and 1.7320 Å.
[b]RCCSD(T)/cc-pCVQZ results based on HF orbitals; the harmonic frequencies calculated at the same level are $\omega_e(ss) = 531.59\ cm^{-1}$, $\omega_e(as) = 1321.17\ cm^{-1}$, and $\omega_e(b) = 42.09\ cm^{-1}$.
[c]The two branches of a $^2\Pi_u$ state.
[d]RCCSD(T) results based on HF orbitals; the harmonic frequencies calculated at the same level are $\omega_e(ss) = 699.98\ cm^{-1}$, $\omega_e(as) = 735.08\ cm^{-1}$, and $\omega_e(b) = 326.15\ cm^{-1}$.
[e]The two branches of a $^4\Pi_u$ state.

of the *in situ* B atoms is in its first excited $^4P$ state, resulting to a


bonding distribution, misleadingly implying a symmetry broken molecule;[8] in other words our ability to distinguish the "left" from the "right" *in situ* B atoms.

The leading equilibrium CASSCF configuration of the AlNAl $\tilde{X}\,^2\Sigma_u^+$ state (counting valence electrons only) and corresponding atomic Mulliken densities are

$$|\tilde{X}\,^2\Sigma_u^+\rangle \approx 0.94|1\sigma_g^2 1\sigma_u^2 2\sigma_g^2 2\sigma_u^1 1\pi_{x,u}^2 1\pi_{y,u}^2\rangle,$$

$$\text{N:}\quad 2s^{1.67}2p_z^{1.24}2p_x^{1.35}2p_y^{1.35},$$

$$\text{Al}_{1,2}:\quad 3s^{1.51}3p_z^{0.45}3p_x^{0.25}3p_y^{0.25}(3d)^{0.16}.$$

The populations are consistent with the previously presented vbL diagrams. The Mulliken charge distribution, $\overset{+0.3}{\text{Al}}-\overset{-0.6}{\text{N}}-\overset{+0.3}{\text{Al}}$, is very similar to that of the diatomic $X\,^3\Pi$ $\overset{+0.3}{\text{Al}}-\overset{-0.3}{\text{N}}$ (AlN).[7]

The dissociation energy of $\text{AlN}-\text{Al}(\tilde{X}\,^2\Sigma_u^+)$ with respect to $\text{AlN}(X\,^3\Pi)+\text{Al}(^2P)$ is $D_e=119.0(118.0)$ kcal/mol at the MRCI(+$Q$) level of theory. Correcting this value with respect to zero point energy (ZPE) calculated at the RCCSD(T) level, i.e.,

$$\begin{aligned}\text{ZPE} &\equiv \text{ZPE(AlNAl)} - \text{ZPE(AlN)}\\ &= \tfrac{1}{2}[\omega_e(\text{ss}) + \omega_e(\text{as}) + 2\omega_e(\text{b})] - \tfrac{1}{2}\omega_e\\ &= \tfrac{1}{2}(533.4 + 1344.5 + 2\times 38.5) - \tfrac{1}{2}758\\ &= 598.5\ \text{cm}^{-1}\quad (=1.71\ \text{kcal/mol}),\end{aligned}$$

we obtain $D_0=117.3(116.3)$ kcal/mol. The MRCI (+$Q$)/cc-pVQZ $D_0=D_e-\omega_e/2$ of $\text{AlN}(X\,^3\Pi)$ is

$$\begin{aligned}D_0 &= 56.3(56.7)\ \text{kcal/mol} - 756/2(750.7/2)\ \text{cm}^{-1}\\ &= 55.2(55.6)\ \text{kcal/mol}.\end{aligned}$$

See also Ref. 7. Therefore the atomization energy of AlNAl is, $\text{AE}=117.3(116.3)+55.2(55.6)=172.5(171.9)$ kcal/mol. The corresponding numbers at the RCCSD(T) level are $D_0(\text{AlN}-\text{Al})=115.7$ kcal/mol, $D_0(\text{Al}-\text{N})=54.5$ kcal/mol, and AE=170.2 kcal/mol. The latter value increases slightly to 171.7 kcal/mol when core-valence correlation effects ($2s^22p^6$ of Al) are included at the RCCSD(T)/cc-pCVQZ. The calculated AE=172 kcal/mol can be considered in fair agreement with the, perhaps, overestimated experimental value of $187.2\pm3.6$ kcal/mol.[2]

The RCCSD(T)/aug-cc-pVQZ adiabatic EA is

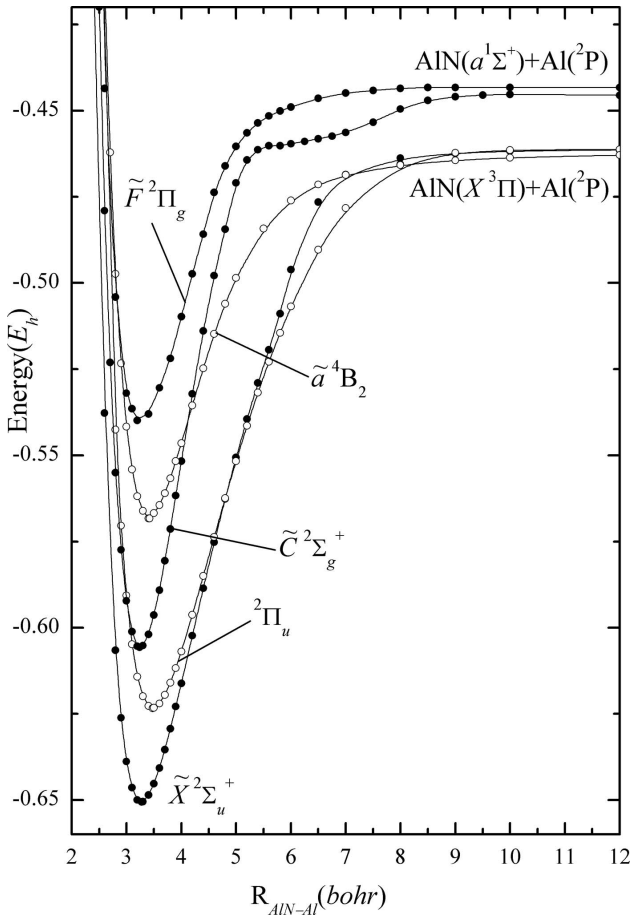


FIG. 1. MRCI/cc-pVQZ AlN–Al dissociation profiles of the $\tilde{X}\,^2\Sigma_u^+$, $^2\Pi_u(\tilde{A}\,^2A_1,\ \tilde{B}\,^2B_1)$, $\tilde{C}\,^2\Sigma_g^+$, $\tilde{a}\,^4B_2$, and $\tilde{F}\,^2\Pi_g$ states. Energies have been shifted by +538.0 $E_h$.

$$\begin{aligned}\text{EA} &= E(\tilde{X}\,^2\Sigma_u^+,\ \text{AlNAl}) + \text{ZPE(AlNAl)}\\ &\quad - [E(\tilde{X}\,^1\Sigma_g^+,\ \text{AlNAl}^-) + \text{ZPE(AlNAl}^-)]\\ &= -538.670\,557\ E_h + 969.72\ \text{cm}^{-1}\\ &\quad - (-538.765\,571\ E_h + 880.21\ \text{cm}^{-1})\\ &= 2.574\ \text{eV},\end{aligned}$$

in perfect agreement with the experimental value of $2.571\pm0.008$ eV of Meloni *et al.*[4] Finally, the RCCSD(T) adiabatic ionization energy (IE) is

$$\begin{aligned}\text{IE} &= E(\tilde{X}\,^1\Sigma_g^+,\ \text{AlNAl}^+) + \text{ZPE(AlNAl}^+)\\ &\quad - [E(\tilde{X}\,^2\Sigma_u^+,\ \text{AlNAl}) + \text{ZPE(AlNAl)}]\\ &= -538.393\,83\ E_h + 1020.2\ \text{cm}^{-1}\\ &\quad - (-538.667\,37\ E_h + 977.5\ \text{cm}^{-1})\\ &= 7.45\ \text{eV}.\end{aligned}$$

Experimentally the first excited state of AlNAl is located $5570\pm970$ cm$^{-1}$ ($15.93\pm2.77$ kcal/mol) above the $\tilde{X}\,^2\Sigma_u^+$ state, assigned to $\tilde{A}\,^2\Pi_u$ symmetry but with the reservation of being "slightly bent."[4]

A linear $^2\Pi$ symmetry of AlNAl can be obtained from the following two degenerate channels at infinity: $Al(^2P;\ M_L=0)+N(^4S)+Al(^2P;\ M_L=\pm 1)$ and $Al(^2P;\ M_L=\pm 1)+N(^4S)+Al(^2P;\ M_L=0)$ or using vbL diagrams:

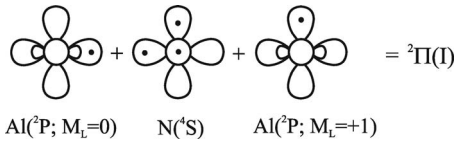


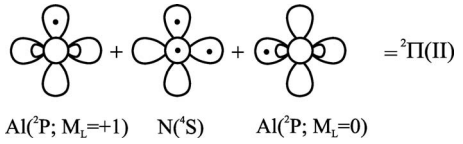


In order to impose the $g$ or $u$ symmetry of the linear AlNAl system, we have to take linear combinations of the $|^2\Pi(\mathrm{I})\rangle$ and $|^2\Pi(\mathrm{II})\rangle$ structures, i.e., $|^2\Pi_{g,u}\rangle = |^2\Pi(\mathrm{I})\rangle \pm |^2\Pi(\mathrm{II})\rangle$, with the +, − signs corresponding to $g$, $u$ symmetries. Diagrammatically,

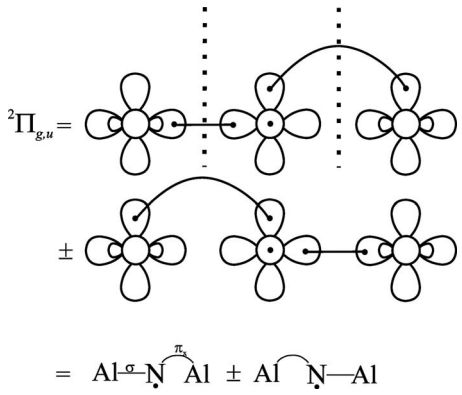


The main $^2\Pi_u$ (valence) CFs and corresponding atomic Mulliken distributions are

$$|^2\Pi_u\rangle \approx 0.94|1\sigma_g^2 1\sigma_u^2 2\sigma_g^2 2\sigma_u^2 1\pi_{x,u}^1 1\pi_{y,u}^2\rangle,$$

$$\mathrm{N}:\quad 2s^{1.75}2p_z^{1.46}2p_x^{0.82}2p_y^{1.49},$$

$$\mathrm{Al}_{1,2}:\quad 3s^{1.78}3p_z^{0.50}3p_x^{0.09}3p_y^{0.22}.$$

Upon pulling apart one of the Al atoms, the inversion symmetry obviously breaks down; the $^2\Pi_u$ dissociates to $AlN(X\ ^3\Pi)+Al(^2P;\ M_L=0)$ (Fig. 1). Note that the *in situ* AlN moiety in the first vbL diagram above, to the right of the first dotted line (to the left of the second dotted line), is in the $X\ ^3\Pi$ ($A\ ^3\Sigma^-$) state, indicating the crucial role of these two AlN states to the formation of the $^2\Pi_u$ symmetry of AlNAl. It should be mentioned at this point that the $X\ ^3\Pi$ and $A\ ^3\Sigma^-$ states of the diatomic AlN are practically degenerate.[7] Of course, *mutatis-mutandis* the same is true for the second vbL diagram after the ± sign. The lack of equivalence between the two Al atoms, $Al(^2P;\ M_L=0)$ and $Al(^2P;\ M_L=\pm 1)$ in either of these two vbL structures, demands the presence of both diagrams to restore the appropriate symmetry and to avoid any artifactual symmetry "breaking effects;" see also Ref. 8.

The bending of the $^2\Pi_u$ removes the twofold degeneracy giving rise to the $\tilde{A}\ ^2A_1$ and $\tilde{B}\ ^2B_1$ states. The $^2B_1$ bending path is repulsive, but the $^2A_1$ leads to the $\tilde{A}\ ^2A_1$ state with $\theta_e=128.82°$ and with a barrier to linearity of 707(571) $cm^{-1}$ [=2.02(1.6) kcal/mol] at the MRCI(+$Q$) level, a rather floppy system in accordance with the observation made in Ref. 4. The energy separation $\Delta E(\tilde{A}\ ^2A_1 \leftarrow \tilde{X}\ ^2\Sigma_u^+)$ is calculated to be 4914(4938) $cm^{-1}$ in agreement with the experimental value of $5570\pm 970$ $cm^{-1}$ of Meloni *et al.*;[4] the corresponding $\tilde{B}\ ^2B_1(^2\Pi_u) \leftarrow \tilde{X}\ ^2\Sigma_u^+$ energy difference is 5621(5509) $cm^{-1}$ (Table I). The MRCI bond distances of the $\tilde{A}\ ^2A_1$ and $\tilde{B}\ ^2B_1(^2\Pi_u)$ states are 1.800 and 1.838 Å, respectively, significantly longer than that of the $\tilde{X}$ state.

Another approach to rationalize the structure of the bent $\tilde{A}\ ^2A_1$ state is to consider the perpendicular attack of the $Al(^2P)$ atom to the diatomic $AlN(X\ ^3\Pi)$. Diagrammatically,

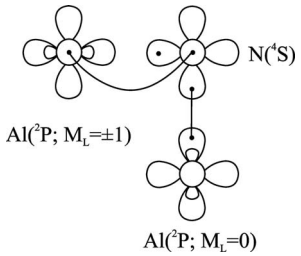


As before the *in situ* "perpendicular" ("horizontal") AlN moiety is in the $A\ ^3\Sigma^-$ ($X\ ^3\Pi$) state, and of course its mirror image with respect to the $C_2$ axis (exchange of the two Al atoms) should be included in the calculation. Note that the equilibrium $\sphericalangle$AlNAl angle $\theta_e=129°$ is practically equal to the mean value of the perpendicular and linear attacks, $(90°+180°)/2=135°$.

We now move to the $\tilde{C}\ ^2\Sigma_g^+$ state located experimentally $10\,490\pm 970$ $cm^{-1}$ above the $\tilde{X}$ state.[4] Our calculated MRCI(+$Q$) value at $r_e=1.715$ Å is $T_e=9850(9811)$ $cm^{-1}$, in good agreement with experiment.[4] Figure 1 displays the dissociative PEC $AlN-Al \rightarrow AlN(a\ ^1\Sigma^+)+Al(^2P;\ M_L=0)$ with $D_e=100.4(100.1)$ kcal/mol.

The prominent equilibrium CASSCF configuration and Mulliken atomic distributions are

$$|\tilde{C}\ ^2\Sigma_g^+\rangle \approx 0.90|1\sigma_g^2 1\sigma_u^2 2\sigma_u^2 2\sigma_g^1 1\pi_{x,u}^2 1\pi_{y,u}^2\rangle,$$

$$\text{N:}\quad 2s^{1.62}2p_z^{1.39}2p_x^{1.32}2p_y^{1.32},$$

$$\text{Al}_{1,2}\text{:}\quad 3s^{1.32}3p_z^{0.57}3p_x^{0.28}3p_y^{0.28}(3d)^{0.17},$$

with a total charge transfer of about $0.6–0.7e^-$ from both Al atoms to N.

The $\tilde{C}\ ^2\Sigma_g^+$ state can be formally derived from the $\tilde{X}\ ^2\Sigma_u^+$ by the $\ldots 2\sigma_g^2 2\sigma_u^1 \ldots \rightarrow \ldots 2\sigma_g^1 2\sigma_u^2 \ldots$ promotion. The atomic populations of the $\tilde{C}\ ^2\Sigma_g^+$ and $\tilde{X}\ ^2\Sigma_u^+$ states are very similar, whereas the $2\sigma_g$ electron of the former is localized on the terminal Al atoms.

Given that the $\tilde{C}\ ^2\Sigma_g^+$ state correlates to $\text{AlN}(a\ ^1\Sigma^+) + \text{Al}(^2P;\ M_L=0)$ and that the $\text{AlN}(a\ ^1\Sigma^+)$ is formed from the $\text{Al}(^4P;\ M_L=0) + \text{N}(^4S)$, we are forced to draw the equilibrium vbL diagram:

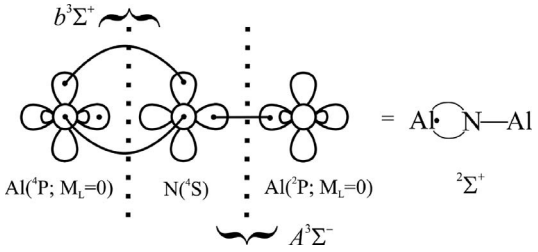


Note, that this diagram is not of $g$ or $u$ symmetry. Including, however, its mirror image, we avoid any artifactual "symmetry breaking" effects, thus obtaining the required inversion symmetry, i.e.,

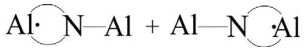


now of $^2\Sigma_g^+$ symmetry. In addition, the vbL diagram explains naturally the linearity of the $\tilde{C}\ ^2\Sigma_g^+$ state, since any nonlinear attack of the Al atom to $\text{AlN}(b\ ^3\Sigma^+)$ does not lead to an attractive interaction and the localization of the $2\sigma_g$ symmetry defining electron on the terminal Al atoms.

The shallow part of the dissociative PEC of the AlNAl $\tilde{C}\ ^2\Sigma_g^+$ state shown in Fig. 1 between 5.2 and 8.0 bohr, is caused by the interaction of the two possible reaction channels $\text{AlN}(b\ ^3\Sigma^+) + \text{Al}(^2P;\ M_L=0)$ and $\text{AlN}(A\ ^3\Sigma^-) + \text{Al}(^4P;\ M_L=0)$ both of $^2\Sigma^+$ symmetry. That the $\tilde{C}\ ^2\Sigma_g^+$ state dissociates to $\text{AlN}(a\ ^1\Sigma^+) + \text{Al}(^2P;\ M_L=0)$ and not to $\text{AlN}(b\ ^3\Sigma^+) + \text{Al}(^2P;\ M_L=0)$ is due to energy reasons: the $a\ ^1\Sigma^+$ state of AlN is lower in energy than the $b\ ^3\Sigma^+$ state by 30.6 kcal/mol.[7]

The next state is of $\tilde{a}\ ^4B_2$ symmetry located 51.6(51.1)[52.5] kcal/mol at the MRCI(+$Q$)[RCCSD(T)] levels of theory, with geometry $r_e=1.812[1.811]$ Å and $\theta_e=90.8°[90.9°]$. The MRCI AlN–Al PEC correlates to $\text{AlN}(X\ ^3\Pi) + \text{Al}(^2P)$ with $D_e=66.5(65.5)$ kcal/mol, or 64.9 kcal/mol at the RCCSD(T) level. The barrier to linearity, $\tilde{a}\ ^4B_2 \rightarrow {}^4\Sigma_u^+$, is calculated to be 26.6 (26.3) kcal/mol.

Assuming that in the $\tilde{a}\ ^4B_2$ state the *in situ* AlN finds itself in the $X\ ^3\Pi$ state the only way to form a strongly bound molecule of $^4B_2$ symmetry is a perpendicular attack of $\text{Al}(^4P)$ to the ground state of $\text{AlN}(X\ ^3\Pi)$. In vbL language (molecule lies on the $yz$ plane):

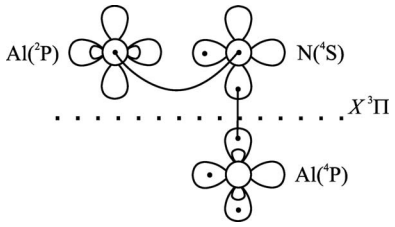


The Al $^4P$ term is experimentally 3.598 eV above the $^2P$ state,[17] and although a similar attack from $\text{Al}(^2P)$ can lead to a quartet state, the strength of the AlN–Al bond (≈67 kcal/mol) precludes such a path. Of course, the equivalence of the two Al atoms requires the structure obtained by exchanging the position of the Al atoms ($C_2$) to be included in the calculation. The main CASSCF equilibrium configuration and the atomic populations (consistent with the vbL diagram) are

$$|\tilde{a}\ ^4B_2\rangle \approx 0.94|1a_1^2 2a_1^2 3a_1^1 4a_1^1 1b_1^2 1b_2^2 2b_2^1\rangle,$$

$$\text{N:}\quad 2s^{1.77}2p_z^{1.11}2p_x^{1.34}2p_y^{1.30},$$

$$\text{Al}_{1,2}\text{:}\quad 3s^{1.28}3p_z^{0.45}3p_x^{0.23}3p_y^{0.55},$$

with a total charge transfer of $0.52e^-$ from both Al atoms to the N atom. We would like to emphasize that the calculated AlNAl angle ($\theta_e=91°$) is in perfect agreement with the above vbL diagram.

The last state to be discussed is the $\tilde{F}\ ^2\Pi_g$ which correlates to $\text{AlN}(a\ ^1\Sigma^+) + \text{Al}(^2P;\ M_L=\pm 1)$; see Fig. 1. At the MRCI(+$Q$) level it lies 24 559(24 076) $\text{cm}^{-1}$ above the ground state at $r_e=1.723$ Å. The leading equilibrium CFs and atomic Mulliken populations are

$$|\tilde{F}\ ^2\Pi_g\rangle \approx 0.80|1\sigma_g^2 1\sigma_u^2 2\sigma_g^2 1\pi_{x,u}^2 1\pi_{x,g}^1 1\pi_{y,u}^2\rangle - 0.49|1\sigma_g^2 1\sigma_u^2 2\sigma_u^2 1\pi_{x,u}^2 1\pi_{x,g}^1 1\pi_{y,u}^2\rangle,$$

$$\text{N:}\quad 2s^{1.65}2p_z^{1.19}2p_x^{1.37}2p_y^{1.37},$$

$$\text{Al}_{1,2}\text{:}\quad 3s^{1.17}3p_z^{0.32}3p_x^{0.72}3p_y^{0.72}.$$

The bonding is faithfully captured by the following vbL diagram, consistent with the CFs and the electron populations

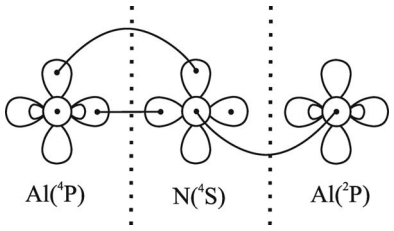


The nondistinguishability of the terminal Al atoms requires its mirror image to be included to ensure the *gerade* ($g$) symmetry. Note that the *in situ* AlN moiety to the left (right) of the second (first) dotted line is of $a\ ^1\Sigma^+$ ($X\ ^3\Pi$) symmetry. The stretching of the AlN–Al bond takes the lower energy path $\mathrm{AlN}(a\ ^1\Sigma^+)+\mathrm{Al}(^2P;\ M_L=\pm 1)$ instead of the $\mathrm{AlN}(X\ ^3\Pi)+\mathrm{Al}(^4P;\ M_L=0)$ higher by 3.1 eV. Finally, the MRCI(+$Q$) AlN–Al dissociation energy with respect to the adiabatic fragments is 60.8 (59.6) kcal/mol.

### B. States $\tilde{D}\ ^2A_1$, $\tilde{E}\ ^2A_1$, $^4\Pi_u(\tilde{b}\ ^4B_1,\ \tilde{c}\ ^4A_1)$, $\tilde{d}\ ^4\Sigma_g^+$, $\tilde{e}\ ^4\Delta_g$, $\tilde{f}\ ^4\Sigma_g^-$, $\tilde{g}\ ^4\Delta_u$, $\tilde{h}\ ^4\Sigma_u^-$, and $\tilde{i}\ ^4\Pi_g$

The ten states above (two doublets and eight quartets) have been studied only around equilibrium. We are certain for the ordering of all states but the $\tilde{b}\ ^4B_1$, $\tilde{c}\ ^4A_1$, and $\tilde{F}\ ^2\Pi_g$ which at the MRCI+$Q$ level their ordering becomes $\tilde{F}\ ^2\Pi_g$, $\tilde{b}\ ^4B_1$, and $\tilde{c}\ ^4A_1$. The $\tilde{b}\ ^4B_1$ and $\tilde{c}\ ^4A_1$ states coalesce to a $^4\Pi_u$ at 180° with $\sphericalangle$AlNAl angles 141° and 180.0°, respectively, and with a barrier to linearity, $\tilde{b}\ ^4B_1 \rightarrow {}^4\Pi_u$ of less than 1 kcal/mol. All ten states are bound with respect to their ground state fragments $\mathrm{AlN}(X\ ^3\Pi)+\mathrm{Al}(^2P)$, with MRCI binding energies ($D_e$) ranging from 61 ($\tilde{D}\ ^2A_1$) to 19 ($\tilde{i}\ ^4\Pi_g$) kcal/mol.

For all states studied in this work a Mulliken charge transfer of about $0.6e^-$ from both Al atoms to N atom is observed; thus we can claim that the AlNAl molecule is ionic enough.

We hope that the present *ab initio* theoretical study of this rather capricious chemical species and the analysis of its bonding could motivate further experimental and theoretical studies.

## ACKNOWLEDGMENTS

We thank Dr. Michael Morse for helpful discussions and for making available to us prior to publication his experimental results on the AlNAl molecule.

[1] K. A. Gingerich, Chem. Commun. **1970**, 441.
[2] G. Meloni and K. A. Gingerich, J. Chem. Phys. **113**, 10978 (2000).
[3] L. Andrews, M. Zhou, G. V. Chertihin, W. D. Bare, and Y. Hannachi, J. Phys. Chem. A **104**, 1656 (2000).
[4] G. Meloni, S. M. Sheehan, B. F. Parsons, and D. M. Neumark, J. Phys. Chem. A **110**, 3527 (2006).
[5] L. Guo, H. S. Wu, and Z. H. Jin, J. Mol. Struct.: THEOCHEM **677**, 105 (2004); Z.-Y. Jiang, W.-J. Ma, H.-S. Wu, and Z.-H. Jin, *ibid.* **678**, 123 (2004); L. Guo, H. S. Wu, and Z. H. Jin, Int. J. Quantum Chem. **103**, 291 (2005).
[6] S. K. Nayak, S. N. Khanna, and P. Jena, Phys. Rev. B **57**, 3787 (1998); A. K. Kandalam, R. Pandey, M. A. Blanco, A. Costales, J. M. Recio, and J. M. Newsam, J. Phys. Chem. B **104**, 4361 (2000); A. Costales, A. K. Kandalam, A. M. Pendás, M. A. Blanco, J. M. Recio, and R. Pandey, *ibid.* **104**, 4368 (2000); B. D. Leskiw, A. W. Castleman, Jr., C. Ashman, and S. N. Khanna, J. Chem. Phys. **114**, 1165 (2001).
[7] A. Kalemos and A. Mavridis, J. Phys. Chem. A **111**, 11221 (2007).
[8] A. Kalemos, T. H. Dunning, Jr., and A. Mavridis, J. Chem. Phys. **120**, 1813 (2004).
[9] T. H. Dunning, Jr., J. Chem. Phys. **90**, 1007 (1989); D. E. Woon and T. H. Dunning, Jr., *ibid.* **98**, 1358 (1993); D. E. Woon and T. H. Dunning, Jr., *ibid.* **103**, 4572 (1995); D. Feller, J. Comput. Chem. **17**, 1571 (1996); K. L. Schuchardt, B. T. Didier, T. Elsethagen, L. Sun, V. Gurumoorthi, J. Chase, J. Li, and T. L. Windus, J. Chem. Inf. Model. **47**, 1045 (2007).
[10] R. A. Kendall, T. H. Dunning, Jr., and R. J. Harrison, J. Chem. Phys. **96**, 6796 (1992).
[11] H.-J. Werner, P. J. Knowles, R. Lindh *et al.*, MOLPRO, Version 2006.1, see http://www.molpro.net.
[12] K. Raghavachari, G. W. Trucks, J. A. Pople, and M. Head-Gordon, Chem. Phys. Lett. **157**, 479 (1989); R. J. Bartlett, J. D. Watts, S. A. Kucharski, and J. Noga, *ibid.* **165**, 513 (1990); **167**, 609E (1990); P. J. Knowles, C. Humpel, and H.-J. Werner, J. Chem. Phys. **99**, 5219 (1993); **112**, 3106E (2000).
[13] K. R. Asmis, T. R. Taylor, and D. M. Neumark, J. Chem. Phys. **111**, 8838 (1999).
[14] S. R. Gwaltney and M. Head-Gordon, Phys. Chem. Chem. Phys. **3**, 4495 (2001).
[15] N. J. Russ, T. D. Crawford, and G. S. Tschumper, J. Chem. Phys. **120**, 7298 (2004).
[16] X. Li and J. Paldus, J. Chem. Phys. **126**, 224304 (2007).
[17] Y. Ralchenko, A. E. Kramida, J. Reader, and NIST ASD Team, NIST Atomic Spectra Database, Version 3.1.5, 2008 (http://physics.nist.gov/asd3) (23 January 2009), National Institute of Standards and Technology, Gaithersburg, MD.